Understanding the Pressure-Induced Emission Enhancement for Triple Fluorescent Compound with Excited-State Intramolecular Proton Transfer

Shayu Li,[†] Qian Wang,[†] Yan Qian,[†] Shuangqing Wang,[†] Yi Li,*[,‡] and Guoqiang Yang*[,†]

Beijing National Laboratory for Molecular Sciences, Key Laboratory of Photochemistry, Institute of Chemistry, Chinese Academy of Sciences, Beijing, 100080, China, and Technical Institute of Physics and Chemistry, Chinese Academy of Sciences, Beijing 100080, China

Received: July 7, 2007; In Final Form: August 30, 2007

An organic compound, *N*-salicylidene-3-hydroxy-4-(benzo[*d*]thiazol-2-yl)phenylamine, with two intramolecular hydrogen bonding and triple fluorescence bands has been synthesized. With increasing pressure, enhanced emission of the triple fluorescence has been observed in succession. Within the pressure region up to 54.2 kbar, the luminescence of the SalHBP solution changed gradually from blue to cyan, until it became almost white. The three bands were assigned to the emission from the enol−enol, keto−enol, and enol−keto excited states of the molecules. The mechanism of the pressure-induced emission enhancement (PIEE) has been investigated with the aid of photophysical measurements and theoretical calculations. The results indicated that the PIEE phenomenon was significantly dependent on factors of hydrogen bond, viscosity, and molecular free volume.

Introduction

High external pressure technology used in probing structural and electronic properties of molecules has been proved as a powerful tool in chemistry, physics, and materials science.[1] Pressure reduces the distance of adjacent molecules and accordingly decreases the volume of a sample. Shorter distance between the molecules enhances possibilities of electronic orbital overlapping and thus changes the orbital energy. Furthermore, shorter distance between the molecules intensely increases the short-range interactions, such as energy transfer with high-order multipole interactions or by Dexter mechanisms.[2] Therefore, for luminescent organic compounds, external pressure will generally result in a decreased emission.[3]

However, a few organic compounds have been investigated for their pressure-induced emission enhancement (PIEE).[4] Although the phenomena were very interesting, the mechanism was explored only in a few reports, possibly for its complexity. Consequently, the underlying causes remained obscure to a large extent. As we know, tens of organic compounds with enhanced emission, caused by changes in the surrounding microenvironment, such as aggregation, viscosity, adsorption, and so forth, have been reported.[5] In most of the explanations in those articles, the enhanced luminescence was caused by limiting the negative factors for the emission that would decrease the fluorescence. We assumed that, if the negative factors were weakened by increasing pressure, the PIEE phenomenon could be observed.

In our previous studies of pressure effects on 2-(2′-hydroxyphenyl)benzoxazole, which is one of the most popular excited-state intramolecular proton transfer (ESIPT) compounds and shows dual fluorescence, it was observed that the high-energy emission was enhanced by external pressure associated with both the low-energy emission and the total emission efficiency decrease.[6] Volume factor had been advised to take responsibility for the unexpected photophysical phenomena.

In this work, a new ESIPT compound, *N*-salicylidene-3-hydroxy-4-(benzo[*d*]thiazol-2-yl)phenylamine (SalHBP), condensed by salicylaldehyde and 2-(4′-amino-2′-hydroxy-phenyl)-benzothiazole, has been synthesized. From the molecular structure, the compound has two ESIPT subunits, which are similar to 2-(2′-hydroxyphenyl)benzothiazole (HBT) and salicylideneaniline (SA). Both subunits have possibility to exhibit enol form and keto form. Thus, three possible emission bands may be possessed by SalHBP molecules: enol−enol (EE) tautomer, keto−enol (KE) tautomer, and enol−keto (EK) tautomer (Scheme 1).

SalHBP molecules were dispersed into 2-methyltetrahydrofuran (meTHF), and its emission behavior was detected. Noticeably, three emission bands were enhanced and tuned by pressure. Photophysical measurements and theoretical studies have been carried out to well understand these specific spectroscopic behaviors.

Experimental Section

Materials. Synthesis of SalHBP. 2-(4′-Amino-2′-hydroxyphenyl)benzothiozole (AHBA) was synthesized using previously published methods.[7]

Salicylidehyde (0.52 mL, 5 mmol) and AHBA (1.21 g, 5 mmol), with a nitrogen inlet and protected from moisture, were added in 30 mL of ethanol to a bath, stirred, and refluxed for 3 h. Light orange yellow precipitates emerged. The bath was cooled, and the precipitates were filtered to give 1.485 g of crude product (yield 85.9%), which was further purified by recrystallization from toluene to get pure bright orange solid, 1.35 g (yield 78%). Mp 244 °C. ^{1}H NMR (400 Hz, chloroform d) $\delta = 11.04$ (1H, s), $\delta = 8.71$ (1H, s), $\delta = 8.02$ (1H, d, $J = 8.06$), $\delta = 7.94$ (1H, d, $J = 7.96$), $\delta = 7.78$ (1H, d, $J = 8.28$), $\delta = 7.48-6.67$ (9H, m), Anal. Calcd for $C_{20}H_{14}N_2O_2S$ (ESI,

* Corresponding authors. (G.Y.) Telephone: 86-10-62569563. Fax: 86-10-62569563. E-mail: gqyang@iccas.ac.cn. (Y.L.) Telephone: 86-10-82543518. Fax: 86-10-82543518. E-mail: yili@mail.ipc.ac.cn.

[†] Beijing National Laboratory for Molecular Sciences.

[‡] Technical Institute of Physics and Chemistry.

10.1021/jp075301a CCC: $37.00
Published on Web 10/27/2007

SCHEME 1: Structure of the Three Excited-State Tautomers of SalHBP (Left) and Energy Diagram of Photoinduced Isomerization Routes of SalHBP (Right)

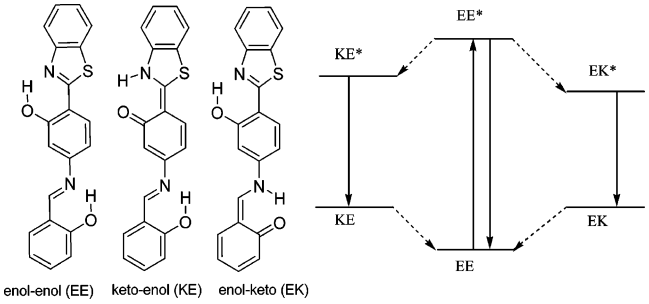

m/*z*: 346.08): C, 0.6935; H, 0.0407; N, 0.0809. Found: C, 0.6912; H, 0.0413; N, 0.0805.

MeTHF was AR grade from Acros.

High-Pressure Spectra Measurement. A Merrill-Bassett diamond anvil cell was used to generate high pressure. The diameter of the hole in the 90-μm-thick stainless steel gasket was about 300 μm. A small chip of ruby was put in the hole to calibrate the pressure by measuring red shift of the fluorescence. For the emission detection, the third harmonic of a pulsed diode pumped nanosecond Nd:YAG laser (355 nm, Amber-5AQ, 20 ns, 7 kHz) and a pulsed diode laser (405 nm, 2 MHz) were used as the excitation source. For the absorption measurement, a Xe lamp was used as light source. The spectra were dispersed with a 0.3-m spectrometer and collected by a photo multiplier. A spectrometer controller module (NCL Electronics Interface, Acton-Research Corporation) and computer were used to record the spectra data. The details of the setup are described in another article.[8]

Low-Temperature Spectra Measurement. Low temperatures were achieved using nitrogen-flow cryostats (Oxford OptistatDN). Temperature was controlled with a precision of 0.1 K Oxford ITC503 temperature controllers. The emission spectrum was recorded with an Edinburgh FLS900 spectrometer, using an excitation wavelength of 355 nm.

meTHF was selected as the solvent for our experiments. It was a versatile and good solvent for most organic compounds. Additionally, it is difficult to crystallize, and therefore transparent glasses can be formed at low temperature or with high pressure.

Theoretical Methods. *Molecular Dynamics (MD) Simulations.* The GROMACS simulation suite[9] was used for the molecular dynamics simulation. Structure parameters of SalHBP were optimized by DFT (B3LYP/6-31G(d)). Point charges were derived according to the RESP procedure.[10] The total system containing nine SalHBP and 702 meTHF molecules was placed in a box with dimensions of $50 \times 50 \times 50$ Å^3 with periodic boundary conditions. Using the conjugate gradient method, we first minimized the total systemic energy. The cutoffs of the van der Waals and electrostatic interactions were set to 12 Å. For a neighbor-list algorithm, a 9 Å cutoff was used. The LINCS algorithm was used to constrain all bonds in the system. To maintain a constant temperature at 300 K, the system was coupled to a thermostat bath adopting the Berendsen method with a time constant $\tau_t = 0.2$ ps. The system was equilibrated in an NPT ensemble using the Parinello−Rahman method with an isotropic pressure coupling having a time constant of $\tau_p = 1.0$ ps. After being equilibrated for 100 ps at pressures of 1 atm with a constant temperature of 300 K, the next simulation was carried out for 3.0 ns with a time step of 0.2 fs. The configuration of the last frame was used for the initial configuration of the next higher pressure simulation until 50 kbar with a step of 5 kbar.

QM Calculations. The ground-state (lowest singlet) geometry of SalHBP was optimized with the Hartree Fock (HF) method. Structures of the three lowest excited-state tautomers (EE, KE, EK) for SalHBP were obtained with the configuration interaction singles (CIS) method. The geometries were fully optimized without symmetry constraints. The calculations of vibration frequencies and normal coordinates were carried out at the CIS structures. Employing the linear coupling model,[11] we investigated the major routes of internal conversion of the three excited states. All these calculations employed all-electron 6-31G(d) basis sets for carbon, hydrogen, oxygen, nitrogen, and sulfur atoms. All calculations described here were performed with the GAUSSIAN suite of programs.[12]

Results

Figure 1a showed pressure-dependent absorption spectra of SalHBP in meTHF solution. At ambient pressure, the solution exhibited a single structureless absorption band peaked at about 372 nm. When the pressure was increased to 20 kbar, the absorbance showed a small bathochromic shift and a slight enhancement. With higher pressure, the band decreased moderately accompanied by a newly appeared absorption band at the shorter wavelength region, which only showed a tail to avoid strong absorption of diamond around 300 nm. Meanwhile, a weak absorption band increased slightly in the longer wavelength region (>420 nm). These changes of absorption spectra implied that the most probable conformation of SalHBP became more conjugated with increased pressure.

The fluorescence spectra of SalHBP in meTHF at various pressures are shown in Figure 1b. At 1 atm, the emission of SalHBP solutions was very weak and showed two peaks with maxima at 420 and 538 nm. When the pressure was increased to about 5 kbar, the emission at 420 nm increased by almost ~3 times, which was a rarely observed phenomenon. Until the pressure increased to ~31 kbar, the fluorescence intensity reached its maximum and afterward began to decrease. At the long wavelength region, a new shoulder emission peak around 500 nm was formed at higher pressure, which could not be detected at ambient pressure. This peak increased immediately after the pressure was enhanced and became obvious at 15.9 kbar and further increased until 31.2 kbar. In the lower energy region, the peak around 538 nm at ambient pressure also enhanced slowly with pressure. With higher pressure up to 38.9 kbar, the peak obviously increased and prevailed the fluorescence of the ~500-nm peak. Note that the iso-emissive point around 530 nm was detected from 31.2 kbar to 54.2 kbar; this implies a conformational transition between two fluorescent species. As can be seen, the ~538-nm emission exhibited a completely different pressure-dependent effect with respect to the ~500-nm emission.

Another interesting phenomenon observed was that SalHBP solution gave a nearly white emission, simultaneously emitting blue, green, and yellow light under high pressure. The photos of this pressure-induced white light are shown in the Supporting Information.

As mentioned earlier, total fluorescence emission of SalHBP solution generally enhanced with increased pressure. In the following section, these emission bands were assigned first, then the major routes of radiationless deactive process were proposed, and finally the origin of PIEE phenomena was investigated.

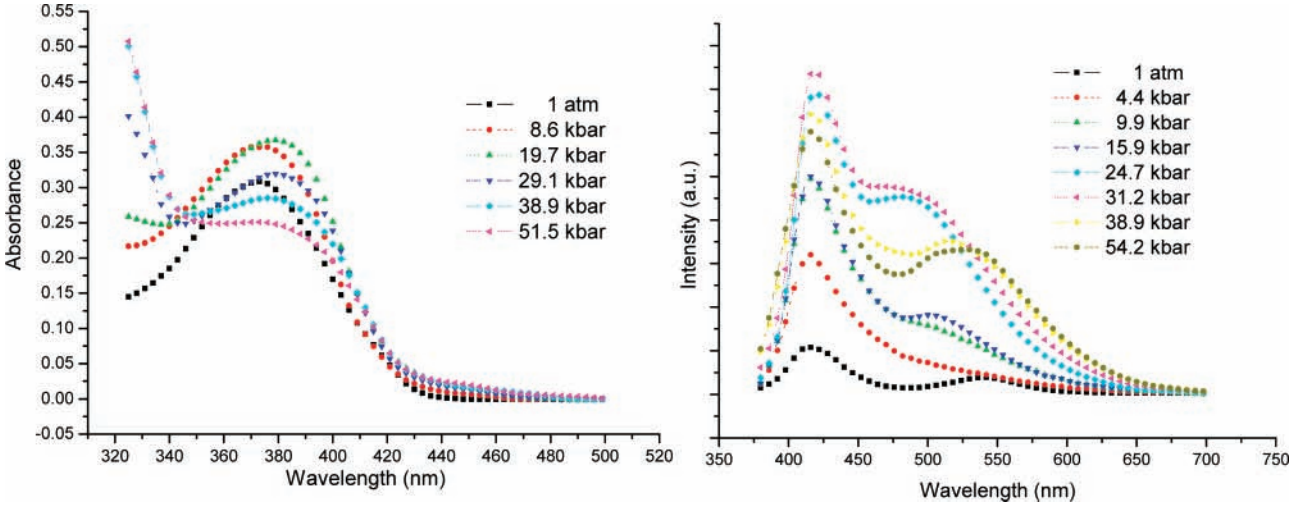

Figure 1. UV−vis absorption spectra (left) and fluorescence emission spectra (right) of SalHBP in meTHF under various pressures (excitation wavelength: 355 nm).

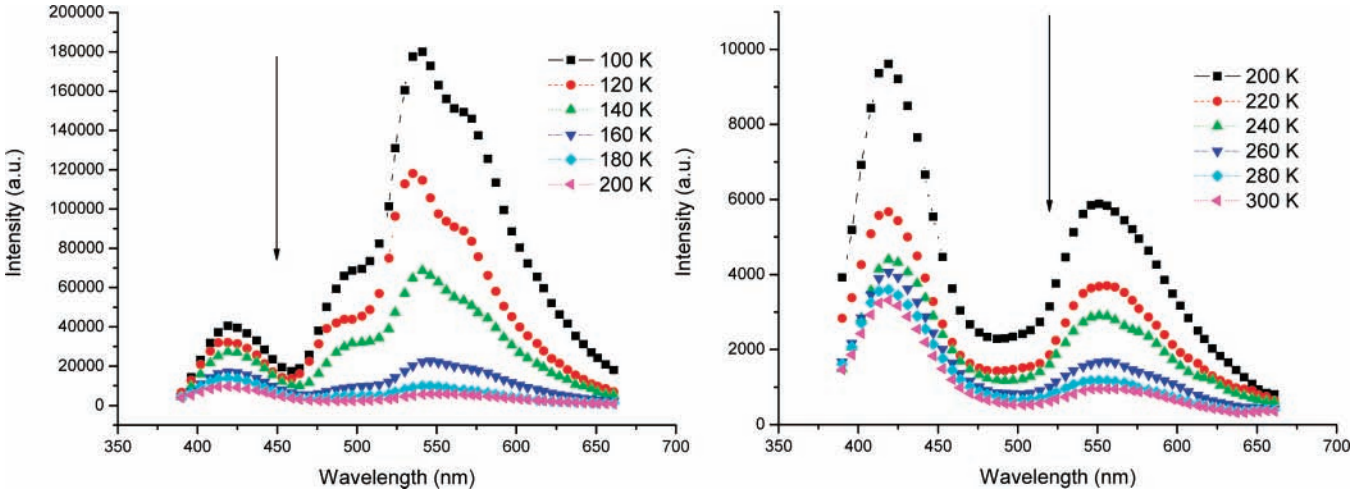

Figure 2. Emission spectra of SalHBP at various temperatures. Left: 100−200 K. Right: 200−300 K (excitation wavelength: 355 nm).

Discussion

A. Assignment of Emission. On the basis of special structure, SalHBP molecules were expected to exhibit three possible emission bands, separately, coming from EE, KE, and EK tautomers. For the emission at 420 nm, the mirror-image relationship and small Stokes shift between the emission and absorption bands indicated that the emission was originated from the EE excited-state form. As for two emissions at the longer wavelength region, the large Stokes shifts revealed that both of them could be assigned to the proton-transfer excited-state characters. As known, ESIPT fluorescence of HBT and SA had been reported to be located at ∼500 and ∼530 nm, respectively.[13] Therefore, emission at ∼500 nm of SalHBP would most probably originate from KE species and another emission at 538 nm would be from EK species.

To understand the assignments of these three emissions, by reason of definition, the fluorescence spectra (Figure 2) of the SalHBP solution were measured at lower temperature (in steps of 20 K from 300 to 100 K). Each emission was intensified continuously with their locations almost unchanged. Below 180 K, the emission band at about 490 nm was obviously observed. The continuous changes in temperature-dependent spectra indicated that at ambient pressure there already existed three emission bands, although the ∼490-nm peak prevailed over the ∼538-nm peak. Figure 3 depicted the normalized excitation spectra of SalHBP monitored at 420, 490, 540, and 560 nm at 100 K. Apparently, the shapes of excitation spectra were similar for the emissions at 420 and 490 nm, with the main excitation

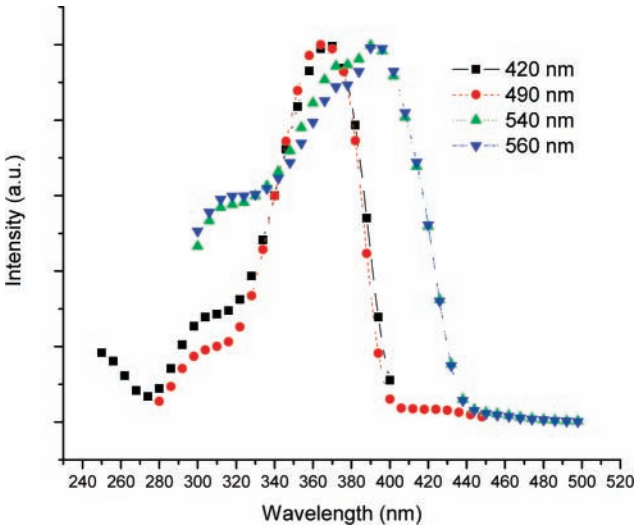

Figure 3. Normalized excitation spectra of SalHBP at 100 K, monitored at 420, 490, 540, and 560 nm.

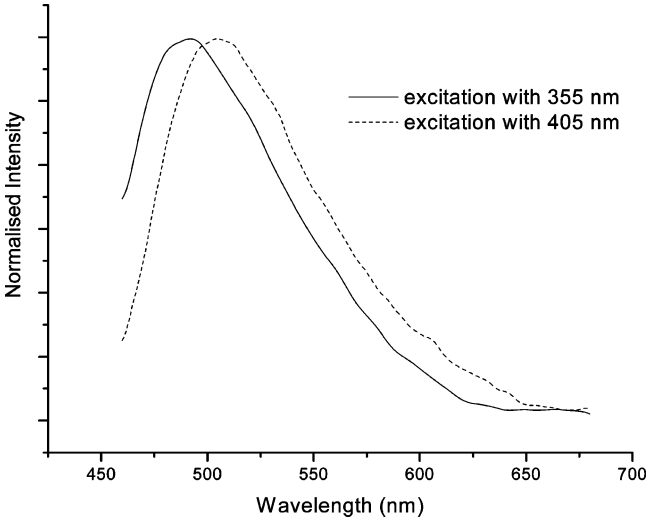

Figure 4. Normalized emission spectra of SalHBP under 25.7 kbar with different excitation wavelengths (with a 460-nm cutoff filter).

maximum at ~360 nm. Excitation spectra of emission at 540 and 560 nm were different from that at 420 and 490 nm and almost unchanged, with the tail region longer than 400 nm. As we know, HBT had no obvious absorption in longer than the 400-nm region, but SA did.[14] Therefore, to the emissions at 540 and 560 nm, they indicated vibronic structure of the emission spectra from EK excited states, while the emission around 490 nm was KE characters.

In addition, the emission spectra of the SalHBP solution under 25.7 kbar had been recorded with the excitation at 355 and 405 nm, as shown in Figure 4. The figure showed a bathochromic shift of the fluorescence spectrum with decreased frequency of the excitation light. This could be considered as a relatively proportional change of emission at ~500 and ~538 nm with different excitation wavelength.

Thus, changes of SalHBP emission under various pressures (Figure 1b) could be depicted simply as follows. With the increase in pressure, the EE emission was enhanced first and then the KE emission increased, and finally the KE emission decreased with increase in the EK emission.

B. Predominant Nonradiative Route of Three Excited States. In general for most luminescent organic molecules, internal conversion (IC), intersystem crossing (ISC) from singlet state to triplet state, and energy transfer to surrounding heterogeneous molecules (ET) were three main nonradiative decay processes. For our compound with EE tautomer, an additional ESIPT process should be involved.

ISC Route. Without heavy atoms in SalHBP molecules, the spin−orbit coupling effect was not apparently contributable to intersystem crossing process. On the other hand, ESIPT was an extremely fast process that only involved singlet states in most cases.[15] No phosphorescence of SalHBP was observed in the 400−900-nm area even at low temperatures in our experiments. As shown in Figure 5, emission decay spectra of SalHBP at 420, 480, 540, and 580 nm at 100 K were detected separately. All the lifetimes were on a nanosecond scale, indicating that these emissions were fluorescence rather than phosphorescence. Therefore, ISC should not be the main radiationless route of the three excited states and could be neglected in this work.

ET Route. On the basis of classical theory descriptions, energy transfer could be classed as Trivial, Förster, or Dexter mechanism.[16] All these mechanisms depended on the overlap integral *J* between the energy donor and acceptor. Since absorbance of meTHF was far from the visible area and located in a high-energy region and the average distance between molecules would be decreased only ~15% under 100 kbar,[17] energy transfer from excited states SalHBP to meTHF should be almost impossible in this work.

Thus, the intermolecular energy transfer route could also be neglected rationally in the SalHBP excited-state nonradiative decay process.

IC Route. Under the displaced harmonic approximation, applying the Born−Oppenheimer adiabatic approximation, the internal conversion radiationless rate was determined by the Huang−Rhys factor (see theoretical and computable details in ref 18). The Huang−Rhys factor was given as:

$$S_j = \frac{\omega_j \Delta Q_j^2}{2\hbar}$$

ΔQ_j was the displacement of *j*th normal mode, and ω_j was the vibrational frequency of *j*th normal mode.

The reorganization energy of *j*th normal mode was

$$\lambda j = S_j \omega_j \hbar$$

In Table 1, the Huang−Rhys factor and the reorganization energy of the three excited-state tautomers between the S_1 and S_0 states with noticeable displacement were given.

a. Enol−Enol Tautomer. The modes with frequency of 1617, 1702, and 1806 cm^{-1} (without correction) had the major contributions to reorganization energy. This indicated that the three vibrations were the most efficient internal conversion deactive routes of S_1 excited state of the EE tautomer. When the vibrational scaled factor was considered to be 0.891 (same value for the HF method) for the CIS method, frequencies of the three modes were obtained as 1440, 1516, and 1609 cm^{-1}, separately. The first mode represented a mixing of aromatic skeletal stretching vibration and C−O (bond order 1.5) stretching vibration. The second and the third modes were the stretching vibrations of aromatic skeletal with various C═N characteristics. In summary, aromatic stretching vibration was the predominant internal conversion route.

b. Keto−Enol Tautomer. The case was so different from EE tautomer. Modes with frequencies of 23, 1427, and 1463 cm^{-1}, which were 21, 1271, and 1303 cm^{-1} after scaled, were the most probable nonradiative deactive routes for the KE tautomer. The computational results indicated that the two bands were located in a high-energy region, belonging to the aromatic C−H in-plane bending motions. It should be pointed out that these in-plane bending motions were mainly localized on the HBT subunit, as shown in Scheme 2. The band at 21 cm^{-1} was assigned to the rotation between the HBT subunit and salicylidene subunit. In addition to the three modes, other modes with large reorganization energy (>100 cm^{-1}) could be assigned to swing, rotating, or bending motions. In addition, stretching motions had a small contribution for total reorganization energy.

c. Enol−Keto Tautomer. The case was different. No modes had a conspicuous contribution to total reorganization energy. There were 13 out of 18 vibrational modes showing apparent reorganization energy, which suggested that several vibrational modes would participate in the IC process. It was noted that the vibrational modes of the aromatic system located on the SA subunit had the most contributions to the reorganization energy, while the vibrational modes correlated to the benzothiazole group almost had few effects on reorganization energy. It was indicated that, in transition of the EK tautomer from S_1 to S_0, conformational modifications were mostly distributed in the SA subunit, shown in Scheme 2.

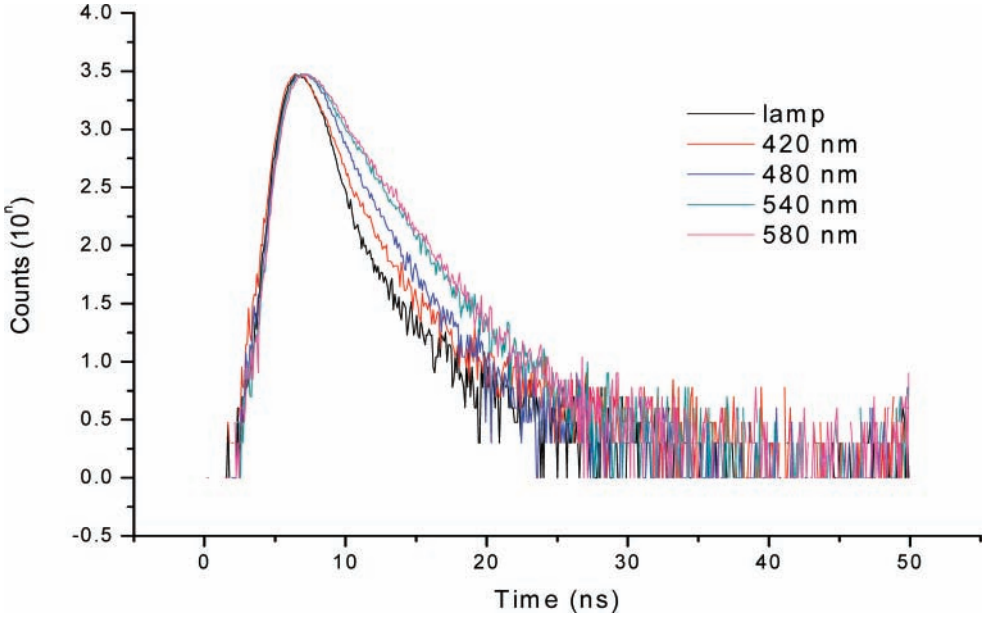

Figure 5. Luminescent decay profiles of SalHBP at 100 K monitored at different wavelengths.

TABLE 1: Huang−Rhys Factors and the Reorganization Energy for the Noticeable Displaced Vibration Modes of Enol−Enol (EE), Keto−Enol (KE), and Enol−Keto (EK) Tautomer of SalHBP

EE			KE			EK		
ω_j (cm^{-1})	S_j	λ_j (cm^{-1})	ω_j (cm^{-1})	S_j	λ_j (cm^{-1})	ω_j (cm^{-1})	S_j	λ_j (cm^{-1})
163	0.54973	90.142	17.7	14.21455	251.68	358	0.27701	99.171
714	0.11650	83.276	23.3	34.7841	809.31	460	0.12248	56.417
858	0.12584	108.04	148	0.91786	136.23	633	0.21109	133.77
1251	0.06691	83.692	223	0.31255	69.614	1112	0.06697	74.491
1348	0.12004	161.92	562	0.10902	61.263	1205	0.21762	262.3
1455	0.04063	59.136	584	0.09257	54.076	1225	0.09817	120.27
1486	0.04026	59.850	1237	0.09133	112.96	1239	0.46333	574.48
1539	0.16093	247.65	1387	0.03865	93.123	1330	0.11143	148.2
1558	0.10511	163.74	1412	0.15788	222.98	1371	0.11075	151.83
1615	0.06296	101.67	1427	0.34821	496.93	1412	0.23607	333.33
1617	0.32701	528.86	1463	0.39803	582.21	1493	0.16354	244.16
1641	0.03506	57.550	1508	0.06356	95.824	1523	0.15450	235.3
1655	0.22229	367.84	1541	0.0422	65.039	1586	0.08164	129.48
1665	0.0564	93.893	1575	0.23911	376.63	1607	0.15026	241.46
1702	0.47474	807.84	1619	0.03346	54.169	1671	0.04604	76.936
1781	0.04343	77.365	1629	0.05848	95.261	1710	0.06161	105.34
1806	0.42745	772.35	1632	0.0349	56.953	1790	0.04033	72.202
3343	0.01691	56.528	3684	0.01447	53.297	3436	0.02782	95.586

SCHEME 2: Main Distributional Scope of Vibrational Modes of Three Excited-State Tautomers of SalHBP That Possess Large Reorganization Energy

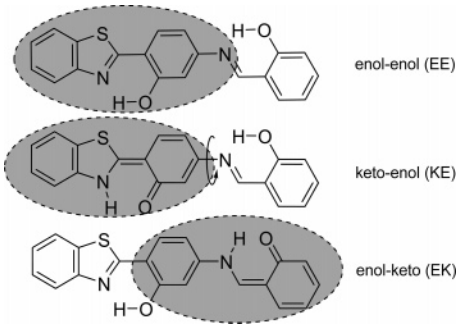

ESIPT Route for the EE Tautomer. ESIPT was a very fast reaction route (k_{ESIPT} is usually $\sim 10^{12}$ s^{-1} for HBT/SA-based molecules[13]) compared to other decay processes.[14] Thus, if involved, it could be estimated as the predominant decay process. Since the ESIPT process could be inhibited by intermolecular H-bond, the efficiency of ESIPT was determined by the population of molecules that could have ESIPT reaction.

As discussed earlier, vibrational motion was the predominant nonradiative route for EK excited-state tautomers, while the rotational motion played the most important role in the deactive process of KE tautomers. As for EE tautomers, the case was more complex: either the ESIPT or IC route would be the possible predominant nonradiative process.

C. PIEE Considerations. Effect of high pressure on vibrational and rotational motions was induced by the fact that pressure could decrease the intra- and intermolecular distances. In general, pressure would have different effects on vibrational and rotational motions. For vibration, the noticeable effects of pressure were shifts of frequency and changes of intensity. Coffer et al. and Li et al. had shown that the pressure dependencies for vibrational modes of organic compounds followed the order $CH_{aromatic}$ stretching > $CC_{aromatic}$ stretching > $CH_{aromatic}$ bending.[19] In common, a more visible influence of pressure on weaker bonds should be observed. For rotation, pressure-induced tight stacking would greatly hinder this motion.

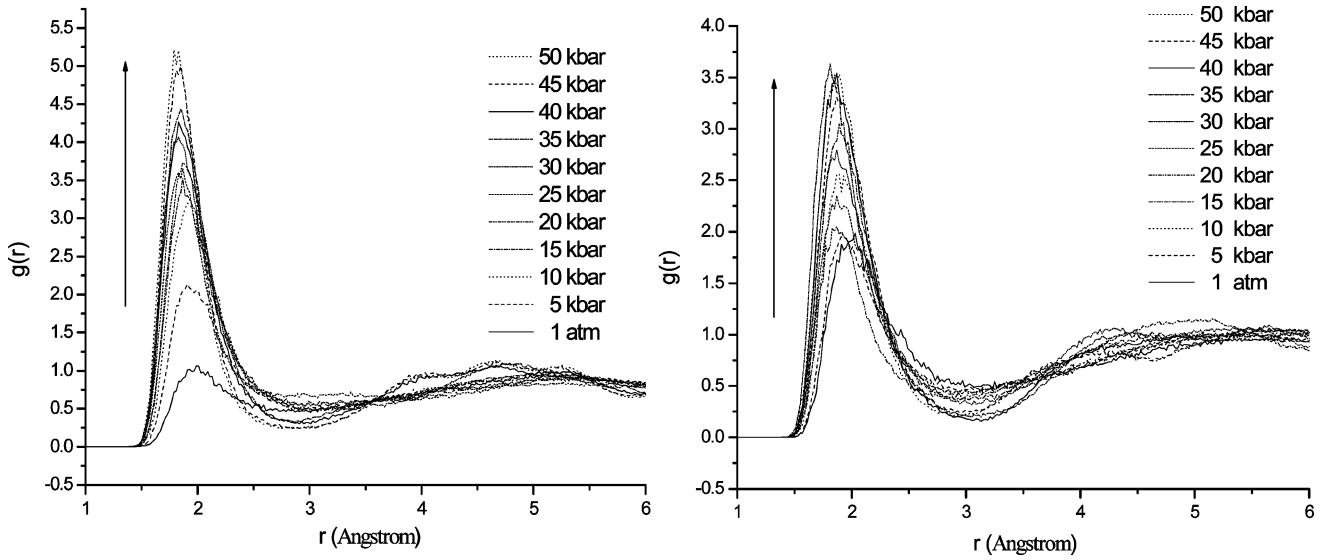

Figure 6. Calculated solute and solvent radial distribution functions for atomic pairs $H_{HBT}\cdots O_{meTHF}$ (left) and $H_{SA}\cdots O_{meTHF}$ (right) under different pressures.

As we know, pressure from 1 atm to 60 kbar could only produce a large change in intermolecular distances but has little effect on intramolecular distances.[17] Therefore, pressure would have a great effect on rotational motions, a modest impact on vibrational motions of external bonds in the molecule, and a small influence on internal bond vibrations positioned inside molecules in our experiments.

As follows, effects of pressure on luminescence of three excited-state tautomers are discussed separately.

Effect of Pressure on Emission of Enol−Enol Tautomers. As summarized in Table 1, aromatic skeletal stretching vibrations were the most predominant internal conversion process for EE tautomers. It was well known that aromatic skeletal stretching vibrations were related to intramolecular atomic distances and located inside the molecule. Pressure in our experiments should have little effect on it. Therefore, pressure-induced changes of ESIPT would be responsible for enhanced emission phenomena. These changes could be considered as a combination of two aspects: ESIPT reaction rate and population of ESIPT reaction molecules.

Several studies on the ESIPT reaction rate with the transient absorption measurements together with detailed theoretical calculations revealed that the low-frequency skeletal vibrations of the molecule make a major contribution to the proton-transfer reaction mechanism.[20] In our experiments, the pressure-induced decreased volume of a system would have a few limitations on the skeletal vibrations of molecules, especially when the pressure was lower than 10 kbar. Since EE emission had been observed, a noticeable enhancement occurred within 10 kbar, in which the intermolecular distances of pure organic system would be reduced merely about 8%.[17] Therefore, changes of ESIPT rate should be negligible for PIEE phenomenon of EE tautomer. Excluding factors of reaction rate, the most possible origin for PIEE of EE tautomer was the increasing population of molecules that could have ESIPT reaction.

The essential condition for ESIPT reaction is the forming of intramolecular hydrogen bonds. When molecules with intramolecular H-bonds were dispersed in solvent molecules with proton acceptor group, a competition between inter- and intramolecular H-bonds would occur inevitably. MD simulations were carried to evaluate this competition case. Because high pressure preventing the rotations was highly sensitive to initial molecular conformation, and with limitation of relatively short duration (3 ns) and size of simulation system compared to the macroscopic time and space size of experiment, it was difficult to obtain accurate data for numbers of inter- and intramolecular H-bonds at various pressure, whereas it was rational to assume the information of H-bonds through analyzing the radial distribution functions (RDFs) since H-bonds are related closely to distances between proton acceptor and donor group.

The calculated RDFs of two possible intermolecular H-bonds, $O_{HBT}-H\cdots O_{meTHF}$ and $O_{SA}-H\cdots O_{meTHF}$, are shown in Figure 6.

For $H_{HBT}\cdots O_{meTHF}$ atom pairs, the simulation reproduced the weak and broad peak at about 1.97 Å under ambient pressure, and the first minimum occurred at 2.96 Å, indicating possible weak hydrogen bond. The location of the peak would be shifted to a shorter distance under high pressure. For instance, the peak was located at 1.91 Å under 10 kbar and 1.80 Å under 50 kbar. Simultaneously, intensity of this peak enlarged rapidly with increasing pressure, particularly when pressure was lower than 10 kbar. The peak with shorter radial distance and higher intensity predicted the possible stronger H-bond interactions.[21] The average coordination numbers calculated by integration from zero to 2.5 Å were 0.53, 1.38, and 1.55 for cases under 1 atm, 10 kbar, and 50 kbar, respectively. More coordination numbers mean more possibility of forming intermolecular H-bonds. Compared to the case of $H_{HBT}\cdots O_{meTHF}$ atom pairs, RDFs of $H_{SA}\cdots O_{meTHF}$ showed a lower response to pressure. At 1 atm and 50 kbar, coordination numbers were calculated as 0.98 and 1.37, respectively.

Taking the facts that the emission around 420 nm was almost independent of salicylidene subunit as stated before, and the computational result about higher response of intermolecular H-bond $O_{HBT}-H\cdots O_{meTHF}$ for pressure, we could conclude that the pressure-induced increase of number for intermolecular H-bonds, which decreased the population of the molecules for the ESIPT process, was the main reason for the PIEE phenomenon of the EE tautomer.

Effect of Pressure on Emission of Keto−Enol Tautomers. As mentioned earlier, rotation and in-plane bending vibration were the most possible radiationless deactivation routes of KE tautomers, especially rotation. In general, increasing the viscosity of the local environment could hinder the free rotation of the single bond. Thus, increasing viscosity of the solvent should enhance the emission of KE tautomers.

TABLE 2: Calculated Viscosity of meTHF under Various Pressures

P (kbar)	1 atm	5	10	15	20	25	30	35	40	45	50
viscosity (cp)	0.7[a]	8.0	30	70	160	210	336	562	1029	1650	10300

[a] 0.536 in *Lange's Handbook of Chemistry*, 16th ed.; Speight, J. G., Ed.; McGraw-Hill: New York, 2005.

Pressure was ever utilized to attain high viscosities of organic solvents at room temperature.[22] Table 2 summarizes the calculated viscosity data of meTHF with pressure by carrying periodic perturbation method.[23] Nonequilibrium NPT simulations were performed with an external Z-dependent acceleration in this method.

Actually, the viscosity of meTHF increased significantly with enhanced pressure. This could be used to interpret the PIEE of the KE tautomer. On the other hand, we noticed that KE emission would decrease with increasing pressure over 31 kbar, which was shown in Figure 1. Considering the fact that an iso-emission point was exhibited around 530 nm, we ascribed this decreased emission to the changes of KE-to-EK tautomer population ratio, which is discussed as follows.

Effect of Pressure on Emission of Enol−Keto Tautomers. We distinguish the effect of pressure as two aspects.

First, as listed in Table 1, some bending and stretching motions of bonds in EK tautomer participated in the nonradiative decay process. Because most of the bonds are located outside the molecule, pressure would do some negative effects on bending motions and decrease internal conversion decay rate more or less. This effect should be more visible with increasing pressure.

Second, it was noticed that the relative intensity of EK emission compared with that of KE emission would increase with longer excitation wavelength as shown in Figure 4. This indicated that the ESIPT precursor of the KE tautomer had a conformation with statistically less conjugation than that of EK tautomer. In other words, the precursor of the EK tautomer should be planar than that of the KE tautomer. Considering that molecules with planar conformation had a relatively smaller molecular volume, and pressure could decrease the occupiable volume of the molecules, high pressure promoted the population of the molecules with planar conformation. This could be corroborated by pressure-induced changes of absorbance in a longer wavelength region (>420 nm), as shown in Figure 1a. Therefore, increasing pressure would increase the population of molecules that could have ESIPT reaction to EK tautomer and decrease the probability that was from EE to KE tautomer simultaneously.

By taking the effects of the above two aspects, high pressure would enhance the emission of EK tautomer significantly.

Conclusions

In contrast to general cases that high pressure would decrease the emission of organic compounds, this work showed an interesting phenomenon about PIEE. Three emission bands of SalHBP were increased in different degrees by increasing pressure. The PIEE mechanisms of the three excited-state tautomers were assigned mainly to (1) pressure increased the quantity of intermolecular H-bonds, (2) pressure increased the viscosity of the system, and (3) pressure tuned the population of the molecules with different conformation. The results gave a novel route to understanding the effect of microenvironment on luminescent efficiency of organic compounds. The pressure-dependent, switchable blue/cyan/white fluorescence made the SalHBP rather unique and possibly suitable for the important applications that include tristable switches and other optical devices.

Acknowledgment. We are grateful to Prof. Z. G. Shuai and Dr. Q. Peng for their kind help on theoretical method. This research was supported by National Natural Science Foundation of China (Grant Nos. 20703049, 20333080, 50303019 and 50221201) and the National Basic Research Program (2007CB808004). The authors also thank the Laboratory of Organic Optoelectronic Functional Materials and Molecular Engineering, Technical Institute of Physics and Chemistry, CAS for their help.

Supporting Information Available: Emission photos of SalHBP under various pressures. This material is available free of charge via the Internet at http://pubs.acs.org.

References and Notes

(1) (a) Chelazzi, D.; Ceppatelli, M.; Santoro, M.; Bini, R. *Nat. Mater.* **2004**, *3*, 470. (b) Schettino, V.; Bini, R. *Phys. Chem. Chem. Phys.* **2003**, *5*, 1951. (c) van Eldik, R.; Ford, P. C. *Adv. Photochem.* **1998**, *24*, 61. (d) Grey, J. K.; Butler, I. S.; Reber, C. *J. Am. Chem. Soc*. **2002**, *124*, 9384. (e) Yersin, H.; Trümbach, D.; Wiedenhofer, H. *Inorg. Chem.* **1999**, *38*, 1411. (f) Horvath-Bordon, E.; Riedel, R.; Zerr, A.; McMillan, P. F.; Auffermann, G.; Prots, Y.; Bronger, W.; Kniep, R.; Kroll, P. *Chem. Soc. Rev.* **2006**, *35*, 987. (g) Mao, W. L.; Mao, H. K.; Hemley, R. J. *Science* **2003**, *302*, 425.

(2) (a) Silbey, R.; Jortner, J.; Rice, S. A. *J. Chem. Phys.* **1965**, *42*, 1515. (b) Dexter, D. L. *J. Chem. Phys.* **1953**, *21*, 836.

(3) (a) Drickamer, H. G. *Annu. Rev. Mater. Sci.* **1990**, *20*, 1. (b) He, L.; Xiong, F.; Li, S.; Gan, Q.; Zhang, G.; Li, Y.; Zhang, B.; Chen, B.; Yang, G. *J. Phys. Chem. B* **2004**, *108*, 7092. (c) Li, H.; Zhong, B.; He, L.; Yang, G.; Li, Y.; Wu, S.; Liu, J. *Appl. Phys. Lett.* **2002**, *80*, 2299.

(4) Dreger, Z. A.; White, J. O.; Drickamer, H. G. *Chem. Phys. Lett.* **1998**, *290*, 399.

(5) (a) An, B.-K.; Kwon, S.-K.; Jung, S.-D.; Park, S. Y. *J. Am. Chem. Soc*. **2002**, *124*, 14410. (b) Tong, H.; Dong, Y.; Häussler, M.; Lam, J. W. Y.; Sung, H. H.-Y.; Williams, I. D.; Sun, J.; Tang, B. Z. *Chem. Commun.* **2006**, *10*, 1133. (c) Li, S.; He, L.; Xiong, F.; Li, Y.; Yang, G. *J. Phys. Chem. B* **2004**, *108*, 10887. (d) Ren, Y.; Lam, J. W. Y.; Dong, Y.; Tang, B. Z.; Wong, K. S. *J. Phys. Chem. B* **2005**, *109*, 1135. (e) Kawasaki, M.; Mine, S. *J. Phys. Chem. B* **2005**, *109*, 17254. (f) Shimizu, K. T.; Woo, W. K.; Fisher, B. R.; Eisler, H. J.; Bawendi, M. G. *Phys. Rev. Lett.* **2002**, *89*, 117401.

(6) Yang, G.; Dreger, Z. A.; Li, Y.; Drickamer, H. G. *J. Phys. Chem. A* **1997**, *101*, 7948.

(7) Ermanno, B.; Piero, S.; Mario, M.; Macro, P. *J. Heterocycl. Chem.* **1983**, *20*, 1517.

(8) Lu, X.; Zhang, H.; Li, Y.; Liu, J.; Yang, G. *Chem. Phys. Lett.* **2001**, *342*, 545.

(9) Lindahl, E.; Hess, B.; Van der spoel, D. *GROMACS 3.0: A package for molecular simulation and trajectory analysis. J. Mol. Model.* **2001**, *7*, 306.

(10) Bayly, C. I.; Cieplak, P.; Cornell, W. D.; Kollman, P A. *J. Phys. Chem.* **1993**, *97*, 10269.

(11) (a) Macak, P.; Luo, Y.; Ågren, H. *Chem. Phys. Lett.* **2000**, *330*, 447. (b) Sharp, T. E.; Rosenstock, M. J. *Chem. Phys.* **1964**, *41*, 3453.

(12) Frisch, M. J.; Trucks, G. W.; Schlegel, H. B.; Scuseria, G. E.; Robb, M. A.; Cheeseman, J. R.; Montgomery, J. A., Jr.; Vreven, T.; Kudin, K. N.; Burant, J. C.; Millam, J. M.; Iyengar, S. S.; Tomasi, J.; Barone, V.; Mennucci, B.; Cossi, M.; Scalmani, G.; Rega, N.; Petersson, G. A.; Nakatsuji, H.; Hada, M.; Ehara, M.; Toyota, K.; Fukuda, R.; Hasegawa, J.; Ishida, M.; Nakajima, T.; Honda, Y.; Kitao, O.; Nakai, H.; Klene, M.; Li, X.; Knox, J. E.; Hratchian, H. P.; Cross, J. B.; Adamo, C.; Jaramillo, J.; Gomperts, R.; Stratmann, R. E.; Yazyev, O.; Austin, A. J.; Cammi, R.; Pomelli, C.; Ochterski, J. W.; Ayala, P. Y.; Morokuma, K.; Voth, G. A.; Salvador, P.; Dannenberg, J. J.; Zakrzewski, V. G.; Dapprich, S.; Daniels, A. D.; Strain, M. C.; Farkas, O.; Malick, D. K.; Rabuck, A. D.; Raghavachari, K.; Foresman, J. B.; Ortiz, J. V.; Cui, Q.; Baboul, A. G.; Clifford, S.; Cioslowski, J.; Stefanov, B. B.; Liu, G.; Liashenko, A.; Piskorz, P.; Komaromi, I.; Martin, R. L.; Fox, D. J.; Keith, T.; Al-Laham, M. A.; Peng, C. Y.; Nanayakkara, A.; Challacombe, M.; Gill, P. M. W.; Johnson, B.; Chen, W.; Wong, M. W.; Gonzalez, C.; Pople, J. A. *Gaussian 03*, revision A.1; Gaussian, Inc.: Pittsburgh, PA, 2003.

(13) (a) Ding, K.; Courtney, S. J.; Strandjord, A. J.; Flom, S.; Friedrich, D.; Barbara, P. F. *J. Phys. Chem.* **1983**, *87*, 1184. (b) Barbara, P. F.; Rentzepis, P. M.; Brus, L. E. *J. Am. Chem. Soc.* **1980**, *102*, 2786.

(14) Becker, R. S.; Lenoble, C.; Zein, A. *J. Phys. Chem.* **1987**, *91*, 3509.
(15) Neuwahl, F. V. R.; Bussotti, L.; Righini, R.; Buntinx, G. *Phys. Chem. Chem. Phys.* **2001**, *3*, 1277.
(16) Turro, N. J. *Modern Molecular Photochemistry;* Benjamin Cummings Publishing: Menlo Park, CA, 1978; Chapter 9.
(17) Okamoto, B. Y.; Drickamer, H. G. *Proc. Natl. Acad. Sci. U.S.A.* **1974**, *71*, 4757.
(18) (a) Yu, G.; Yin, S.; Liu, Y.; Chen, J.; Xu, X.; Sun, X.; Ma, D.; Zhan, X.; Peng, Q.; Shuai, Z.; Tang, B.; Zhu, D.; Fang, W.; Luo, Y. *J. Am. Chem. Soc.* **2005**, *127*, 6335 and references therein. (b) Yin, S.; Peng, Q.; Shuai, Z.; Fang, W.; Wang, Y.-H.; Luo, Y. *Phys. Rev. B* **2006**, *73*, 205409.
(19) (a) Coffer, J. L.; Drickamer, H. G.; Park, J. T.; Roginski, R. T.; Shapley, J. R. *J. Phys. Chem.* **1990**, *94*, 1981. (b) Li, H. Q.; Butler, I. S.; Harrod, J. F. *Organometallics* **1993**, *12*, 4553.
(20) Ziółek, M.; Kubicki, J.; Maciejewski, A.; Naskrecki, R.; Grabowska, A. *J. Chem. Phys.* **2006**, *124*, 124518.
(21) (a) Astley, T.; Birch, G. G.; Drew, M. G. B.; Rodger, P. M.; Wilden, G. R. H. *J. Comput. Chem.* **1998**, *19*, 363. (b) Carver, T. J.; Drew, M. G. B.; Rodger, P. M. *Phys. Chem. Chem. Phys.* **1999**, *1*, 1807.
(22) Herbst, C. A.; Cook, R. L.; King, H. E. *J. Non-Cryst. Solids* **1994**, *172*−*174*, 265.
(23) Hess, B. *J. Chem. Phys.* **2002**, *116*, 209.